1

Introduction to Polyoxometalates

Daniela Flores and Carlos M. Granadeiro

University of Porto, LAQV/REQUIMTE, Department of Chemistry and Biochemistry, Faculty of Sciences, Rua do Campo Alegre, s/n, Porto 4169-007, Portugal

1.1 Introduction

Polyoxometalates (POMs) represent a captivating and unique class of nanoscale metal–oxide clusters, boasting remarkable structural and chemical versatility, making them a sought-after choice across diverse scientific domains [1–3], namely biomedicine, catalysis, colloid science, electronic or magnetic devices, functional materials, nanotechnology, sensors and surfaces [4, 5]. The exploration of these materials dates back to the 1826 discovery by Berzelius of the ammonium salt of $[PMo_{12}O_{40}]^{3-}$. However, it was not until 1933, when Keggin conducted the first structural determination of the tungsten analogue $[PW_{12}O_{40}]^{3-}$ over a century later, that their structural intricacies began to be unveiled [6]. The scientific community has devoted considerable effort and time to the structural characterization of these intriguing compounds, and so the potential applications of POMs only began to be truly explored after the late 1970s.

POMs are inorganic clusters composed of metallic centres, frequently in their highest oxidation state (M = V, Mo, W, Nb and Ta), named the addenda atoms, connected by bridging or terminal oxygen atoms. Currently, there are a large number of known POMs structures with diverse architectures and distinct compositions. In order to establish correlations between their highly symmetric structures, physical properties and reactivity, POMs are typically divided into two main categories: isopolyanions and heteropolyanions (Figure 1.1) [7].

Isopolyanions, with the general formula $[M_xO_y]^{m-}$, are composed of a metal–oxide framework where the addenda atom is a singular transition-metal ion from group V or VI surrounded by oxygen atoms. Heteropolyanions, represented by the general formula $[X_zM_xO_y]^{n-}$ with $z \leq x$, contain an additional atom (X) named heteroatom. In POM structures, heteroatoms are typically elements from the p-block (X = P, Si, Al, Ga, Ge) but also from the d-block (X = Fe, Co, Ni, Zn), which are located at the centre of a M_xO_y shell [8].

The spatial arrangement of POMs can be visualized as packed arrays of polyhedral MO_x units, typically MO_6 octahedra or, more rarely, MO_5 pyramidal units.

Applied Polyoxometalate-based Electrocatalysis, First Edition. Edited by Diana M. Fernandes.

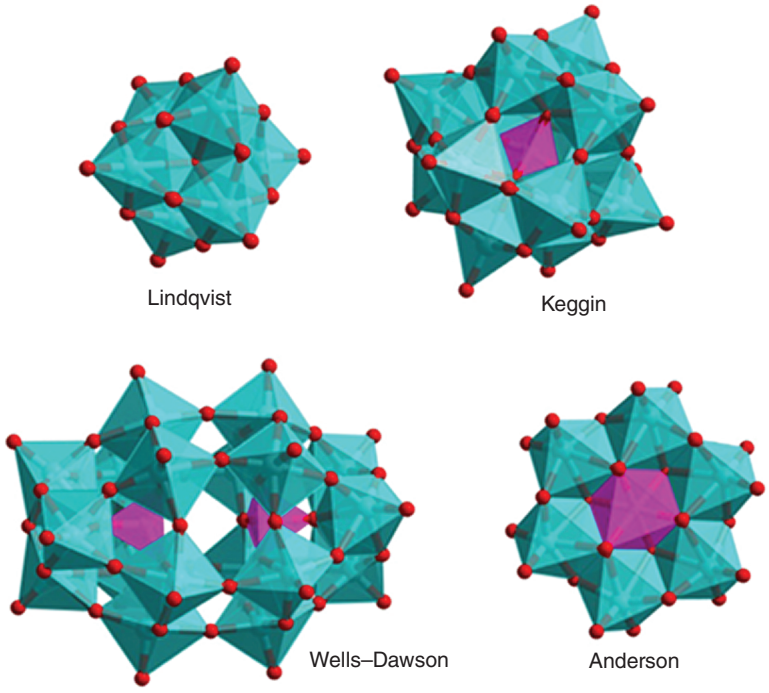

Figure 1.1 Structural representation of the most common POM categories: the Lindqvist isopolyanion ($[M_6O_{19}]^{n-}$), and the heteropolyanions Keggin-($[XM_{12}O_{40}]^{m-}$), Wells–Dawson-($[X_2M_{18}O_{62}]^{w-}$) and Anderson-type ($[XM_6O_{24}]^{n-}$) anions. MO_x: light blue; X: purple; O: red. Source: Granadeiro et al. [4]/with permission of Elsevier.

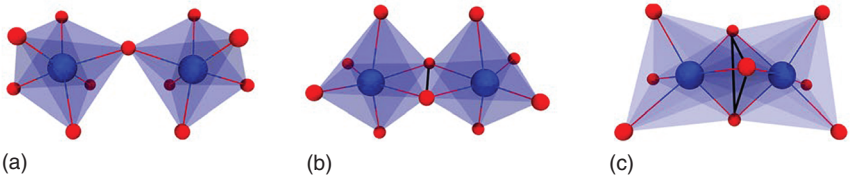

Figure 1.2 Polyhedral and ball-and-stick representation of the different types of MO_6 connectivity in POMs: (a) corner-shared, (b) edge-shared and (c) face-shared octahedra. Source: Bijelic and Rompel [9]/Springer Nature/CC BY 4.0.

These units act as building blocks in the construction of multiple architectures by connecting between themselves and sharing edges, corners or faces (Figure 1.2) [10]. Based on this, the oxygen atoms in a POM structure can be classified according to their position (Figure 1.3). The oxygen atom connected to the heteroatom is denoted as O_a, O_b and O_c represent corner- and edge-sharing atoms, while the unshared (terminal) oxygen atom is denoted as O_d [12].

The vast number of POM structures is further broadened by the use of more than one type of M addenda atoms (mixed-addenda anions) or by structural modification through the removal of one or more MO_x groups (lacunary anions). The formation of lacunary POM anions (Figure 1.4) is achieved by varying the

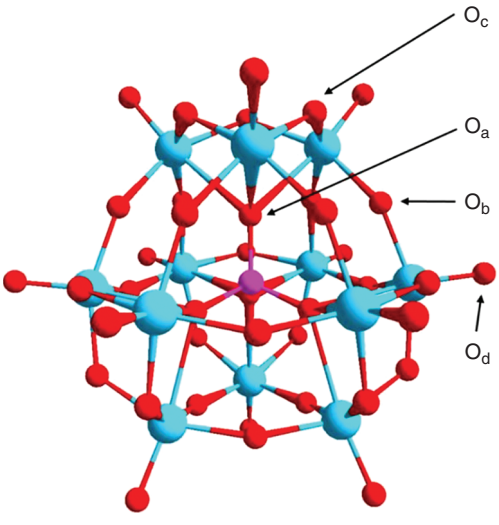

Figure 1.3 Ball-and-stick representation of the Keggin anions with the different type of oxygen atoms: O_a: heteroatom-connected oxygen; O_b: corner-shared oxygen; O_c: edge-shared oxygen; O_d: terminal oxygen. Source: Zheng et al. [11]/The Royal Society of Chemistry/CC BY 3.0.

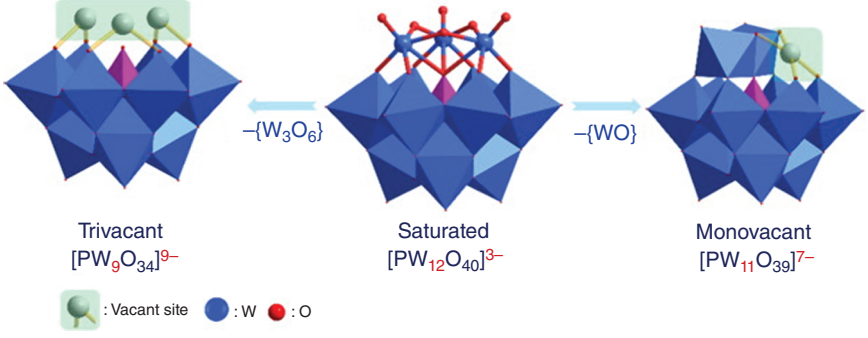

Figure 1.4 Polyhedral and ball-and-stick representations of the formation of mono- and trilacunary (vacant) Keggin-type POMs. Source: Bao et al. [13]/with permission of Elsevier.

experimental conditions, such as temperature, pH or precursors, which are frequently used to achieve enhanced reactivity and superior mechanical properties [14, 15]. The obtained empty lacuna with free oxygen atoms leads the anion to act as a tetradentate or pentadentate ligand capable of coordinating to any electrophilic species, typically lanthanide or transition-metal ions [5]. By doing so, unprecedented structures have been obtained by the connection of two (or more) known anions, including the formation of supramolecular POM structures.

1.2 Polyoxometalate Structures

1.2.1 Synthetic Methodologies

The synthesis of POM structures is relatively straightforward, typically involving an acidic solution containing relevant metal oxide anions. This can be achieved by

following two main methodologies: (i) one-pot synthesis and (ii) building block method. In the one-pot synthesis, a condensation reaction takes place between simple metal salts and heteroanions. However, this approach demands the precise control over several key parameters, namely the choice of reducing agent, concentration and type of metal oxide anion, heteroatom type and concentration, ionic strength, pH, presence of additional ligands and reaction temperature [16]. In the building block method, lacunary anions, obtained by removal of MO_x groups from parent POM anions, act as precursors to build bulkier and more complex POM structures [17]. The lacunary derivatives, typically prepared by controlled hydrolysis of parent POM solutions, contain nucleophilic oxygen centres and will act as multidentate ligands in the construction of discrete larger clusters or even polymeric networks through coordination to electrophilic species [18]. The more efficient and elegant approach of the building block method has led to the exponential growth of novel POM structures with increasingly complex arrangements, higher number of functionalities and distinct physico-chemical properties, enlarging the application fields of POMs [19–21].

1.2.2 Lindqvist Structure

The Lindqvist structure is the most representative example of isopolyanions with the general formula $[M_6O_{19}]^{n-}$ with M = W, Mo, Cr and Nb. The monolacunary Lindqvist polyoxotungstate unit $[W_5O_{18}]^{6-}$ has been extensively used as building block by coordination to lanthanide and transition-metal ions. In particular, decatungstates composed of two $[W_5O_{18}]^{6-}$ units coordinated to a central lanthanide ion [22] have shown peculiar properties motivating their synthesis and application in photoluminescence, catalysis, medical imaging and as single-molecule magnets (SMM) [23–27]. In these compounds, with the general formula $[Ln(W_5O_{18})_2]^{9-}$, the lanthanide ion is coordinated to eight oxygen atoms exhibiting a square antiprismatic geometry [28]. The $[Eu(W_5O_{18})_2]^{9-}$ anion is among the most studied POMs due to its exceptionally high quantum yield arising from the highly efficient energy transfer process from the O → W charge transfer band to the lanthanide ion [29].

1.2.3 Keggin Structure

The Keggin structure, with the general formula $[XM_{12}O_{40}]^{n-}$, stands as the most well-known heteropolyanion featuring tetrahedrally coordinated heteroatoms and four trimetallic M_3O_3 groups arranged around a central XO_4 tetrahedron [30]. The Keggin anion exhibits five rotational isomers (α, β, γ, δ and ε) resulting from consecutive 60° rotations of each M_3O_3 unit (Figure 1.5) [7].

Keggin anions, through controlled alkaline hydrolysis, are also able to form lacunary species by removing one or more MO_x groups from the plenary structure. The monolacunary $[XM_{11}O_{39}]^{(n+4)-}$ Keggin anion is able to coordinate to trivalent (or even tetravalent) metallic cations through the available oxygen atoms in the lacuna

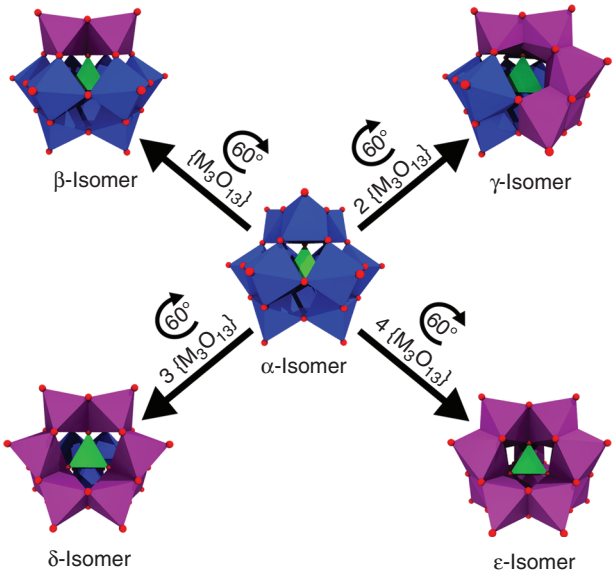

Figure 1.5 Polyhedral representation of the rotational isomers of the Keggin anions. Source: Bijelic and Rompel [9]/Springer Nature/CC BY 4.0.

[4]. These monolacunary anions typically originate as 1 : 1 $[XM_{11}M'(L)O_{39}]^{n-}$ or 1 : 2 $[M'(XM_{11}O_{39})_2]^{n-}$ complexes. The 1 : 1 complexes are mainly obtained when the metallic cation (M′) is a transition-metal or p-group element. For these complexes, L represents a monodentate ligand (generally a water molecule) necessary to complete the octahedral coordination of M′. Bulkier metallic cations (e.g. lanthanide ions) tend to coordinate to two monolacunary units forming a 1 : 2 complex [31]. Nevertheless, a few examples can be found in the literature reporting 1 : 1 complexes with lanthanide ions [17, 19, 32]. The formation of 2 : 2 Keggin-type complexes is even rarer, although some crystalline structures have already been reported, namely $[\{Ln(H_2O)_3(\alpha\text{-}PW_{11}O_{39})\}_2]^{6-}$ with Ln(III) = Nd, Gd (Figure 1.6) [33].

Trilacunary Keggin anions $[XM_9O_{34}]^{(n+6)-}$, obtained from the removal of three MO^{4+} units, are also commonly used in the preparation of POM structures. The removal of the three MO^{4+} units can be from octahedra sharing a corner (A-type) or sharing an edge (B-type) (Figure 1.7).

Several crystalline determinations of POM structures using trilacunary Keggin anions as building blocks have been described, mostly using tungstoarsenate, tungstophosphate, tungstoantimonate and tungstosilicate moieties [34–37].

The major area of application for Keggin-based POMs has been catalysis, mainly oxidative reactions with alcohols, alkenes and aldehydes [38, 39], as well as in the fields of electro- and photocatalysis [40]. Besides, europium-containing Keggin POMs have also shown interesting luminescent features [29], gadolinium-containing Keggin POMs have exhibited promising features as MRI contrast agents [41], while holmium and erbium analogues have been explored as SMMs [25].

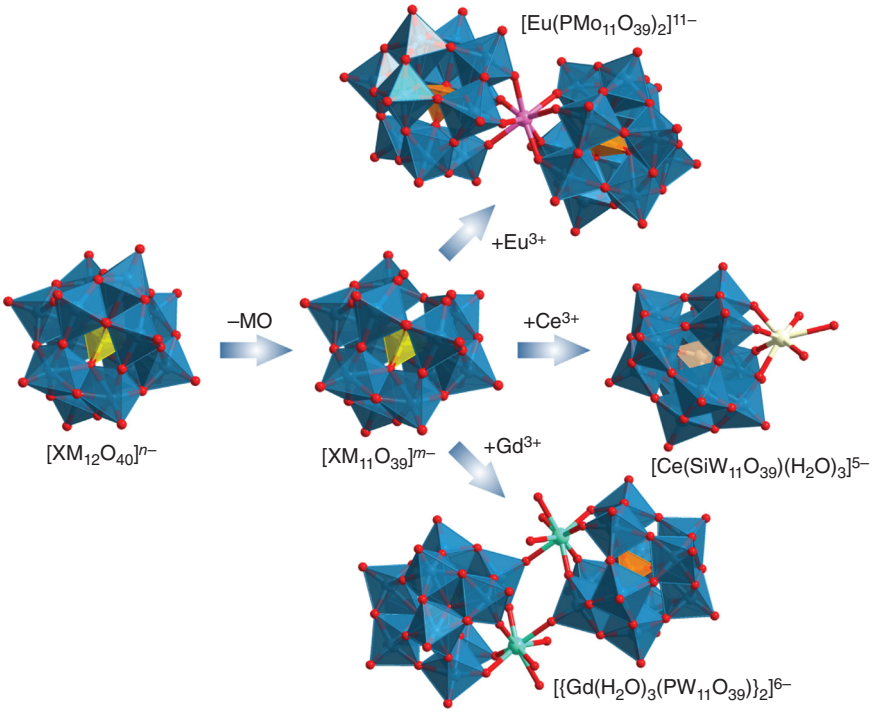

Figure 1.6 Polyhedral representation of the Keggin-type complexes: 1 : 2 $[Eu(PMo_{11}O_{39})_2]^{11-}$, 1 : 1 $[Ce(SiW_{11}O_{39})(H_2O)_3]^{5-}$ and 2 : 2 anionic $[\{Gd(H_2O)_3(\alpha\text{-}PW_{11}O_{39})\}_2]^{6-}$. Source: Granadeiro et al. [21]/with permission of Elsevier.

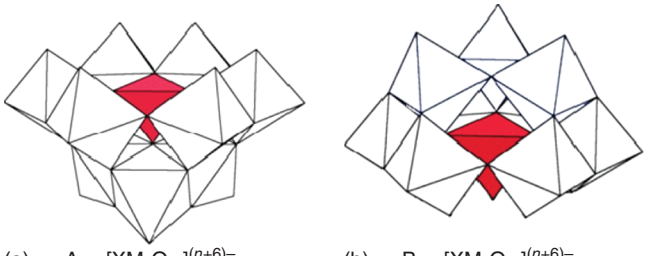

Figure 1.7 Polyhedral representation of the A- and B-type isomers of the Keggin trilacunary structure. (a) A-α-$[XM_9O_{34}]^{(n+6)}$ and (b) B-α-$[XM_9O_{34}]^{(n+6)}$.

1.2.4 Wells–Dawson Structure

The Wells–Dawson structure, with the general formula $[X_2M_{18}O_{62}]^{n-}$, consists of a diamagnetic anion composed of 18 MO_6 octahedra sharing corners and edges with the heteroatoms occupying the tetrahedral positions. Depending on the orientation of the two top M_3O_3 units, the Wells–Dawson structure displays three rotational isomers (α, β or γ) (Figure 1.8) [43]. Wells–Dawson anions can also form lacunary

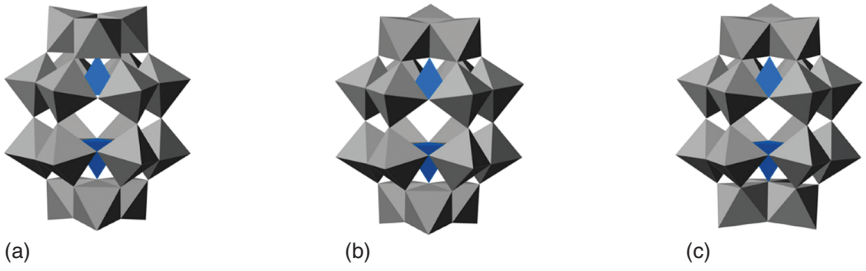

Figure 1.8 Polyhedral representation of the rotational isomers of the Wells–Dawson anions. (a) α-Wells–Dawson, (b) β-Wells–Dawson, and (c) γ-Wells–Dawson. Source: Matsunaga et al. [42]/MDPI/CC BY 4.0.

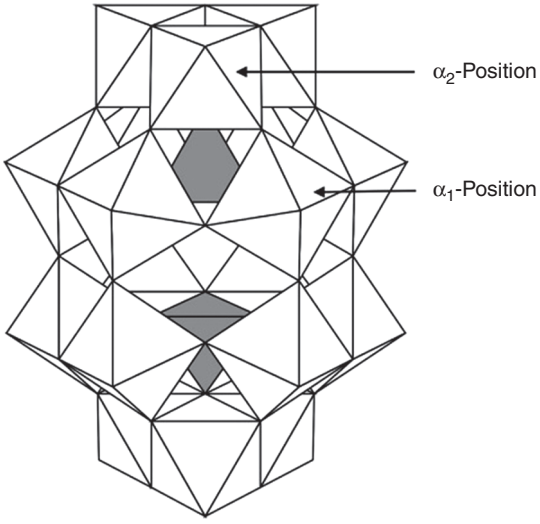

Figure 1.9 Polyhedral representation of the positional isomers of the α-monolacunary Wells–Dawson structure. Source: Huang et al. [45]/MDPI/CC BY 4.0.

derivatives by removing one or more MO_x groups from the parent structure. In the case of isomers of lacunary species, it is necessary to distinguish between the different isomers by specifying the location of the lacuna [44]. Considering the α-isomer, if the lacuna is located in the equatorial region, the isomer is denoted as α_1, while if the lacuna is located at the top, the isomer is α_2 (Figure 1.9).

Monolacunary Wells–Dawson anions have also been used as building blocks for the preparation of monomeric 1 : 1 or dimeric 1 : 2 or 2 : 2 complexes by coordination to metallic cations [46]. The metallic centre in 2 : 2 dimers can coordinate to an oxygen atom of another unit in a 'cap-to-cap' or 'cap-to-belt' arrangement depending on whether the oxygen atom is located at the top or at the equatorial region, respectively [47, 48].

Numerous Wells–Dawson-based POM structures have been reported to date, consisting of either monomeric or dimeric complexes mainly containing α-isomers due to their higher stability when compared with the other isomers [46, 49, 50]. Among α-isomers, the number of crystalline reports dealing with the α_2-isomer is

considerably higher than with the chiral α_1-isomer due to the minor stability of the latter [51, 52].

Several other Wells–Dawson-based structures have been reported using either multilacunary (di-, tri- and hexalacunary) or even mixed isomers as building blocks [53–56]. For instance, Pope and co-workers have combined different Wells–Dawson isomers to prepare the α_1,α_2-mixed $[Ce(\alpha_1\text{-}P_2W_{17}O_{61})(\alpha_2\text{-}P_2W_{17}O_{61})]^{17-}$ [57], while Hill and co-workers reported the use of two trilacunary $[\alpha\text{-}P_2W_{15}O_{56}]^{12-}$ Wells–Dawson derivatives linked by an ytterbium-containing cluster [58].

Wells–Dawson-based POMs have been mainly applied in the fields of catalysis and magnetism [59–61]. Despite the relatively weak emission of lanthanide-containing Wells–Dawson POMs, some reports can be found dealing with their application in photoluminescence [62–64]. Granadeiro et al. proposed the synthesis of organic–inorganic hybrids composed of lanthanide-containing $[\alpha_2\text{-}P_2W_{17}O_{61}]^{10-}$ Wells–Dawson units and 3-hydroxypicolinic acid [62]. In these hybrids, sensitization of the lanthanide luminescence could be more efficiently achieved via the organic ligands leading to an enhancement of the global quantum efficiency.

1.2.5 Anderson–Evans Structure

The Anderson–Evans structure (commonly referred to simply as Anderson), with the general formula $[XM_6O_{24}]^{n-}$, consists in a planar ring arrangement composed of a central heteroatom with octahedral geometry XO_6 surrounded by six MO_6 edge-sharing octahedral [65]. In this structure, there are three distinct coordination modes of oxygen atoms: triple-bridged (μ_3-O), double-bridged (μ_2-O) and terminal (O_d) oxygen atoms. Anderson-type structures can be classified according to the protonation of the oxygen atoms (Figure 1.10) [66, 67]. The non-protonated A-type Anderson with the general formula $[X^{n+}M_6O_{24}]^{(12-n)-}$ and the protonated B-type Anderson in which the protons are located on the μ_3-O atoms around the heteroatom with the formula $[X^{n+}(OH)_6M_6O_{18}]^{(6-n)-}$.

In the Anderson-type structure, despite the addenda atoms being practically limited to W or Mo, nearly all first-row transition-metals have been reported as heteroatoms. Moreover, several other elements, such as metalloids and post-transition-

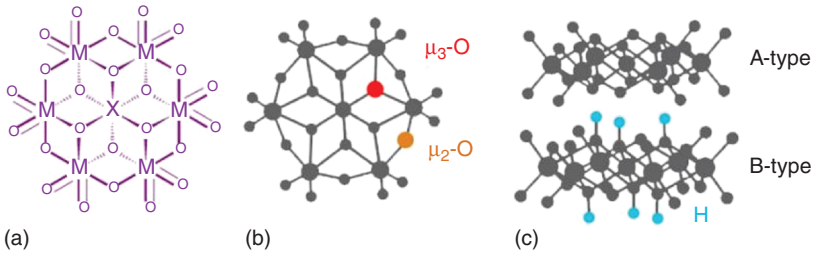

Figure 1.10 Structure of the Anderson-type POM (a), ball-and-stick representation of the Anderson structure highlighting the different coordination of oxygen atoms (b) and the different types (A- or B-) according to the protonation of oxygen atoms (c). Source: Wei et al. [65]/MDPI/CC BY 4.0.

metals (Al, Ga, Sb, Te), have also been used as heteroatoms in Anderson-type structures. Nevertheless, there is a predominance in the number of reported crystalline structures using $[Cr(OH)_6Mo_6O_{18}]^{3-}$, $[TeMo_6O_{24}]^{6-}$, $[AlMo_6(OH)_6O_{18}]^{3-}$ and $[Co(OH)_6Mo_6O_{18}]^{3-}$ as building units [68, 69].

The physico-chemical properties of the Anderson-type POM are mainly governed by the type of heteroatom present in the structure [14, 70]. These anions have been mainly applied in the fields of photochromism, photocatalysis, biomedicine and magnetism [71, 72].

1.2.6 Preyssler Structure

The Preyssler-type POM is a bulky heteropolyoxotungstophosphate with the general formula $[XP_5W_{30}O_{110}]^{14-}$ first described by Preyssler in 1970 [73]. It is composed of five $[PW_6O_{22}]^{9-}$ units linked together in a cyclic arrangement forming an internal cavity occupied by an encrypted cation. In this structure, the presence of water molecules coordinated to the cation displaces it outside the equatorial plane of the framework [74]. Although the original cationic element is sodium, several other crystalline Preyssler structures have been reported using different central cations typically achieved by cationic-exchange procedures. Pope et al. reported a series of novel Preyssler-type structures by replacement of the central sodium cation by trivalent lanthanides as well as tetravalent Ce and U [75]. However, the crystalline structure for these compounds was only determined a few years later for the europium-exchanged $([Eu(OH_2)P_5W_{30}O_{110}])^{14-}$ anion [76]. Kortz and co-workers described the direct synthesis of the silver-analogue $[AgP_5W_{30}O_{110}]^{14-}$ Preyssler structure by solvothermal and microwave-assisted synthesis [77]. Wang and co-workers prepared the first non-phosphate Preyssler-type POM by using tetrahedral $\{SO_4\}$ group in the structure leading to $[XS_5W_{30}O_{110}]^{14-}$ with $X = Na^+$ or K^+ [78] (Figure 1.11).

The central cationic centre strongly influences the physico-chemical properties of the Preyssler-type structure, ultimately determining their fields of application. The europium-containing analogue has been mainly investigated with promising results in luminescent, photo- and electrochromic applications [64, 80–84]. Sodium-

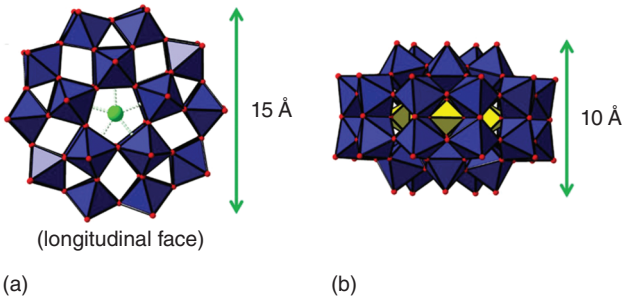

Figure 1.11 Polyhedral representation of the Preyssler-type POM: top view (a) and side view (b). Source: Leclerc et al. [79]/MDPI/CC BY 4.0.

and silver-containing Preyssler POMs have been successfully tested as antibacterial, antitumour and antiviral agents [85–89].

1.2.7 Other POM Structures

Besides the more traditional and well-known POM structures, several other examples of POM compounds have been reported. Dexter and Silverton described the crystal structure of a dodecamolybdocerate anion with the general formula $[Ce^{IV}Mo_{12}O_{42}]^{8-}$ [90]. The central position is occupied by cerium heteroatom surrounded by 12 face-sharing MoO_6 octahedra. The development of novel synthetic methods and the technological advances in the field of crystallography have undoubtedly contributed to the appearance of unprecedented POM structures with high nuclearities and increased complexity. Several authors have described the synthesis of POM-based compounds by combining different types of anions. In these mixed-type POM structures, generally prepared under hydro-/solvothermal synthesis, distinct smaller POM fragments (e.g. Lindqvist, Keggin) are joined together, typically using metallic clusters as linkers, to produce bulkier and more complex POM arrangements [21]. For instance, Yamase et al. reported numerous mixed-POM structures by combining trilacunary Keggin $[B\text{-}\alpha\text{-}SbW_9O_{33}]^{9-}$ and monolacunary Lindqvist $[W_5O_{18}]^{6-}$ units as building blocks [91–94].

The appealing physico-chemical properties and peculiar structural arrangements of high-nuclearity POM clusters have led to the development of supramolecular structures that can reach nanometric dimensions, generally referred as giant POMs [95, 96]. The construction of these nanosized assemblies relies on the use of metal cations, namely lanthanide ions and transition-metal ions, as linkers to assemble the smaller individual POM units [97]. Pope and co-workers have reported the synthesis and crystallographic determination of the wheel-shaped $[As_{12}Ce_{16}(H_2O)_{36}W_{148}O_{524}]^{76-}$ with a diameter of c. 4 nm [15]. This giant cyclic structure contains 148 tungsten atoms and combines $[B\text{-}\alpha\text{-}AsW_9O_{33}]^{9-}$ and $[W_5O_{18}]^{6-}$ units linked together by cerium clusters. Müller et al. have described several wheel-shaped giant POM structures which reach nanometric dimensions [98–100]. Interestingly, in the crystalline structure of the cyclic $[Mo_{120}O_{366}(H_2O)_{48}H_{12}\{Pr(H_2O)_5\}_6]^{6-}$ anion, six $\{Pr(H_2O)_5\}^{3+}$ fragments occupy the positions of $\{Mo\}^{2+}$ units ultimately influencing the shape and size of the ring. Recent and comprehensive reviews dealing with the plethora of nanosized high-nuclearity POM wheels have been reported highlighting their recent applications in the fields of catalysis, magnetism, luminescence, proton conductivity and molecular recognition [101, 102].

1.3 POM-based Composites and Materials

Over the years, the unique and intriguing physico-chemical properties of POMs have raised enormous interest in the scientific community. The structural diversity, coordination flexibility and extensive possibility of elemental compositions in

POMs make them potential candidates in a wide range of application fields. Nevertheless, the direct application of POMs in specific applications can uncover some limitations/drawbacks, such as low surface area, leaching, poor conductivity, mechanical and thermal stabilities and difficulty to remove from reactional media. Several strategies have been employed to overcome such issues by preparing POM-based composites and materials with enhanced processability and reinforced stability. The main strategies to develop POM-based composites and materials are (i) self-assembled hybrids using cationic surfactants, (ii) embedment in thin films/membranes, (iii) immobilization on support materials.

The properties of POMs can be tuned by replacing the original counterions with cationic surfactants resulting in surfactant-encapsulated Polyoxometalates (SEPs). The surfactant molecules surround the POM moieties and create a protective hydrophobic environment which promotes the preservation of the POM properties (Figure 1.12). The use of long alkyl chain surfactants has proved to be a useful strategy to prepare SEPs with enhanced features for applications in catalysis and luminescence. SEPs containing specific surfactants have been reported to behave as heterogeneous catalysts enabling their recovery and consequent recycling from the reactional media [103, 104]. Regarding luminescence, the hydrophobic environment in SEPs avoids the well-known luminescence quenching by water molecules and allows for lanthanide-containing POMs to preserve their emission even in aqueous media [81, 105]. Some of the most widely used surfactants to prepare SEPs include dimethyldioctadecylammonium (DODA), dodecyltrimethylammonium (DDTA), dodecyl(11-methacryloyloxyundecyl)dimethylammonium (DMDA) and di(11-hydroxyundecyl)dimethylammonium bromide (DOHDA).

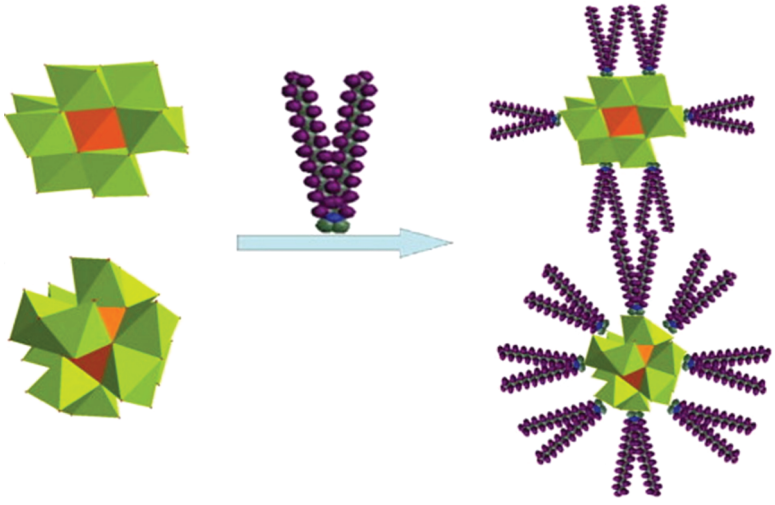

Figure 1.12 Formation of surfactant-encapsulated POM (SEPs) through replacement of counterions by cationic surfactants exemplified for $(DODA)_6[MnMo_9O_{32}]\cdot 16H_2O$ (top) and $(DODA)_8[CeMo_{12}O^{42}]\cdot 9H_2O$ (bottom). Source: Jia et al. [103]/with permission of Elsevier.

Recently, a different methodology to prepare surfactant-assembled POMs has been reported, named 'complex coacervate core micelles' (C3Ms) [106, 107]. These materials, assembled by electrostatic interactions, rely on neutral–cationic block copolymers. In C3Ms, the neutral segments of the copolymer surround the micellar core composed of its cationic segments and the anionic POM units.

The preparation of POM-embedded thin films and membranes is one of the most used approaches to prepare POM-based materials. Numerous stable and ordered films/membranes containing POM moieties have been reported owing to the solubility of POMs in distinct organic solvents [4]. The main techniques for POM-embedded films and membranes are Langmuir–Blodgett (LB), layer-by-layer (LbL), solvent-casting and spin-coating [108, 109]. The LB technique starts with the formation of a cationic surfactant monolayer on the surface of an aqueous dilute POM solution. Through immersion of a solid support, POM-embedded thin films can be obtained with controllable orientation and thickness [110]. The LbL technique involves the alternate immersion of a substrate in a cationic polyelectrolyte solution followed by immersion in anionic POM solutions, resulting in electrostatically assembled multilayered films [111]. POM-based thin films typically use poly(allylamine hydrochloride) (PAH), polyethyleneimine (PEI) and poly(styrenesulphonate) (PSS) as polyelectrolytes. Solvent-casting is a straightforward method for preparing POM-based films and membranes, involving dispersion of POMs in a volatile solvent and direct casting onto a flat surface [112, 113]. Despite being one of the most used methods, it has great limitations regarding homogeneity and thickness of the prepared films. Spin-coating is a highly versatile technique that allows to prepare pure homogeneous POM films with controlled thickness and relies on centrifugal force to spread the coating over a substrate [114]. Recently, electrospinning has proved to be an extremely promising and versatile technique for the production of POM-based films and membranes. Electrospun fibrous meshes are produced by applying a specific voltage to a tip through which POM-dispersed polymeric solutions are ejected and collected on a rotating drum [115]. Electrospinning allows to successfully overcome the processability, stability and scalability issues associated with the previous techniques while permitting a precise control over morphology and orientation by simply adjusting the experimental parameters [116] (Figure 1.13).

The majority of reports dealing with the preparation of POM-based composites relies on the immobilization of POM moieties on solid supports, namely mesoporous silica, layered double hydroxides (LDHs) and metal–organic frameworks (MOFs). A considerable number of POM anions have been immobilized on mesoporous silica frameworks, especially for catalytic and luminescence applications [117]. Mesoporous silica is a highly suitable candidate for support owing to its high internal surface area, stability, optical transparency and possibility to tune pore size and surface functionalization [118]. In particular, MCM-41 and SBA-15 ordered mesoporous silica materials have been extensively used for the immobilization of POMs [119]. In order to assure efficient POM anchoring, mesoporous silica materials are typically functionalized with different organosilanes which allow to minimize the leaching of the POM species [39, 120]. LDHs or anionic clays

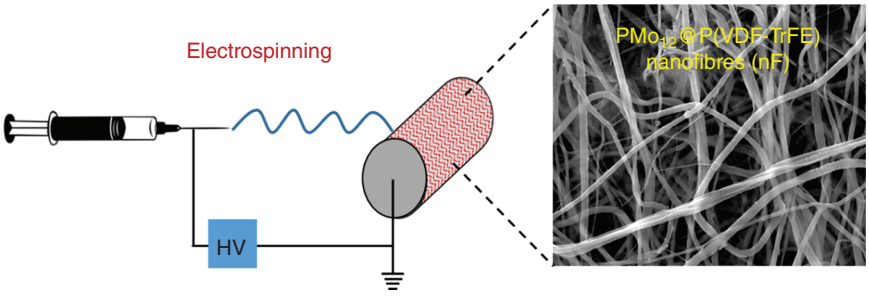

Figure 1.13 Representation of POM-containing electrospun fibre meshes exemplified for the Keggin phosphomolybdate embedded in PVDF polymeric matrix. Source: Reproduced with permission of Mirante et al. [116]/Royal Society of Chemistry.

are lamellar materials composed of positively charged layers intercalated with anionic species [121]. In LDHs, a wide range of negatively charged species can be intercalated by anionic exchange due to the weak interactions between layers. The great interest in LDHs as POM supports is due to their layered structure that allows for a wide range of POM anions with different sizes and spatial orientations to be intercalated by adjustment of the LDH interlayer distance [122]. Most of the reports dealing with POM-intercalated LDHs aim at their application as heterogeneous catalysts [123–125], although some reports can be found in the field of photoluminescence [126, 127]. MOFs are highly porous multidimensional crystalline structures obtained through coordination of metallic centres with organic ligands. The exceptionally high surface area, permanent porosity, post-synthetic functionalization and high thermal stability of MOFs soon attracted the scientific interest in these materials as solid supports able to efficiently accommodate a wide array of active species (including POMs) [128, 129]. The preparation of POM@MOF composites generally follows different synthetic pathways: (i) impregnation of MOF frameworks with POM solutions, (ii) 'bottle-around-the-ship' through the in situ synthesis of MOFs in the presence of POMs and (iii) 'ship-in-a-bottle' by the direct POM synthesis onto the MOF channels and cages [21]. The preparation of POM@MOF composites has proven to be a very efficient strategy for the heterogenization of some of the most catalytically active POM species. The MIL-type MOF structures, especially MIL-100 and MIL-101, have been particularly chosen due to their adequately large pore sizes with accessible channels for POM accommodation as well as their remarkable chemical and thermal robustness [130–134]. A few reports also show the promising potential of POM@MOF composites in optical sensing and electrocatalytic applications [135–138].

1.4 Conclusions

Over the last decades, POM chemistry has gained immense attention from the scientific community on the account of its peculiar physico-chemical properties and the virtually infinite combination of structural arrangements and chemical

compositions. This chapter provides a comprehensive summary of the traditional POM structures (Lindqvist-, Keggin-, Wells–Dawson-, Preyssler-type, Anderson–Evans and others) together with some of the related properties and synthesis methodologies. The application of these POM arrangements as building blocks in the construction of more intricate POM-based architectures has also been addressed. The main strategies for the production of POM-based materials, namely surfactant encapsulation, formation of thin films/membranes and immobilization on support materials, were also reviewed.

The more conventional application areas of POMs (catalysis, luminescence, magnetism) have initially triggered much of the research work and interest in POM chemistry. Nevertheless, the technological progress leading to the development of advanced characterization techniques and innovative synthetic strategies allowed to significantly expand the range of applications and highlight the potential of POMs in several emerging areas.

This chapter intends to highlight that, despite the increasing number and type of POM-based composites and materials reported over the last years, there are still plenty of innovative opportunities to be explored in the field of POM chemistry. Considering the unique features of POMs herein revisited, it is expected that, in the near future, increasingly more industrial and technological applications will be developed employing POM-based materials and devices.

References

1 Pope, M.T. and Müller, A. (1991). Polyoxometalate chemistry: an old field with new dimensions in several disciplines. *Angew. Chem. Int. Ed. Engl.* 30: 34–48.

2 Li, F., Xu, L., Wei, Y. et al. (2006). Lanthanide-containing and bridged polyoxometalate chains: syntheses, crystal structures and magnetic properties. *Inorg. Chim. Acta* 359: 3795–3799.

3 Misra, A., Kozma, K., Streb, C., and Nyman, M. (2020). Beyond charge balance: counter-cations in polyoxometalate chemistry. *Angew. Chem. Int. Ed.* 59: 596–612.

4 Granadeiro, C.M., de Castro, B., Balula, S.S., and Cunha-Silva, L. (2013). Lanthanopolyoxometalates: from the structure of polyanions to the design of functional materials. *Polyhedron* 52: 10–24.

5 Das, V., Kaushik, R., and Hussain, F. (2020). Heterometallic 3d-4f polyoxometalates: an emerging field with structural diversity to multiple applications. *Coord. Chem. Rev.* 413: 213271.

6 Keggin, J.F. (1933). Structure of the molecule of 12-phosphotungstic acid. *Nature* 131: 908–909.

7 Coronado, E., Borrás-Almenar, J.J., Müller, A., and Pope, M. (ed.) (2003). *Polyoxometalate Molecular Science*. Dordrecht: Springer.

8 Yurchenko, É.N., Detusheva, L.G., Solov'eva, L.P. et al. (1992). Identification of type heteropolyantions and isopolyanions from the vibrational spectra of their crystalline salts. *J. Struct. Chem.* 33: 373–382.

9 Bijelic, A. and Rompel, A. (2018). Polyoxometalates: more than a phasing tool in protein crystallography. *ChemTexts* 4: 10.

10 Kondinski, A. (2016). On the isomer problem of mixed–addenda and heterogroup–substituted polyoxometalates. Doctoral dissertation. Jacobs University Bremen.

11 Zheng, Z., Zhou, Q., Li, M., and Yin, P. (2019). Poly(ethylene glycol) nanocomposites of sub-nanometer metal oxide clusters for dynamic semi-solid proton conductive electrolytes. *Chem. Sci.* 10: 7333–7339.

12 Braunstein, L.A.O.P. and Raithby, P.R. (ed.) (2008). *Metal Clusters in Chemistry*. Wiley-VCH.

13 Bao, W., Huang, T., Wang, C. et al. (2022). Controlled synthesis of efficient NiWS active phases derived from lacunary polyoxometalate and the application in hydrodesulfurization. *J. Catal.* 413: 374–387.

14 Gouzerh, P. and Proust, A. (1998). Main-group element, organic, and organometallic derivatives of polyoxometalates. *Chem. Rev.* 98: 77–112.

15 Wassermann, K., Dickman, M.H., and Pope, M.T. (1997). Self-assembly of supramolecular polyoxometalates: the compact, water-soluble heteropolytungstate anion $[AsCe(H_2O)_{36}W_{148}O_{524}]^{76-}$. *Angew. Chem. Int. Ed. Engl.* 36: 1445–1448.

16 Long, D.-L., Tsunashima, R., and Cronin, L. (2010). Polyoxometalates: building blocks for functional nanoscale systems. *Angew. Chem. Int. Ed.* 49: 1736–1758.

17 Sadakane, M., Dickman, M.H., and Pope, M.T. (2000). Controlled assembly of polyoxometalate chains from lacunary building blocks and lanthanide-cation linkers. *Angew. Chem. Int. Ed.* 39: 2914–2916.

18 Mirzaei, M., Eshtiagh-Hosseini, H., Alipour, M., and Frontera, A. (2014). Recent developments in the crystal engineering of diverse coordination modes (0–12) for Keggin-type polyoxometalates in hybrid inorganic–organic architectures. *Coord. Chem. Rev.* 275: 1–18.

19 Mialane, P., Lisnard, L., Mallard, A. et al. (2003). Solid-state and solution studies of $\{Ln_n(SiW_{11}O_{39})\}$ polyoxoanions: an example of building block condensation dependent on the nature of the rare earth. *Inorg. Chem.* 42: 2102–2108.

20 Xuan, W., Pow, R., Long, D.-L., and Cronin, L. (2017). Exploring the molecular growth of two gigantic half-closed polyoxometalate clusters $\{Mo_{180}\}$ and $\{Mo_{130}Ce_6\}$. *Angew. Chem. Int. Ed.* 56: 9727–9731.

21 Granadeiro, C.M., Julião, D., Ribeiro, S.O. et al. (2023). Recent advances in lanthanide-coordinated polyoxometalates: from structural overview to functional materials. *Coord. Chem. Rev.* 476: 214914.

22 Peacock, R.D. and Weakley, T.J.R. (1971). Heteropolytungstate complexes of the lanthanide elements. Part I. Preparation and reactions. *J. Chem. Soc. A* 1836–1839.

23 Granadeiro, C.M., Ferreira, R.A.S., Soares-Santos, P.C.R. et al. (2010). Lanthanopolyoxotungstates in silica nanoparticles: multi-wavelength photoluminescent core/shell materials. *J. Mater. Chem.* 20: 3313–3318.

24 Carvalho, R.F.S., Pereira, G.A.L., Rocha, J. et al. (2021). Lanthanopolyoxometalate-silica core/shell nanoparticles as potential MRI contrast agents. *Eur. J. Inorg. Chem.* 2021: 3458–3465.

25 AlDamen, M.A., Cardona-Serra, S., Clemente-Juan, J.M. et al. (2009). Mononuclear lanthanide single molecule magnets based on the polyoxometalates $[Ln(W_5O_{18})_2]^{9-}$ and $[Ln(\beta_2\text{-}SiW_{11}O_{39})_2]^{13-}$($Ln^{III}$ = Tb, Dy, Ho, Er, Tm, and Yb). *Inorg. Chem.* 48: 3467–3479.

26 Fernandes, S., Mirante, F., Castro, B.d. et al. (2022). Lindqvist versus Keggin-type polyoxometalates as catalysts for effective desulfurization of fuels. *Catalysts* 12: 581.

27 Granadeiro, C.M., Ribeiro, S.O., Kaczmarek, A.M. et al. (2016). A novel red emitting material based on polyoxometalate@periodic mesoporous organosilica. *Microporous Mesoporous Mater.* 234: 248–256.

28 Mariichak, O.Y., Ignatyeva, V.V., Baumer, V.N. et al. (2020). Heteropoly decatungstolanthanidates(III) with Peacock–Weakley type anion: synthesis and crystal structure of isostructural salts $Na_9[Ln(W_5O_{18})_2]\cdot 35H_2O$ (Ln = Gd, Er). *J. Chem. Crystallogr.* 50: 255–266.

29 Binnemans, K. (2009). Lanthanide-based luminescent hybrid materials. *Chem. Rev.* 109: 4283–4374.

30 Pope, M.T. (2013). Happy birthday Keggin structure! *Eur. J. Inorg. Chem.* 2013: 1561–1561.

31 Müller, A., Peters, F., Pope, M.T., and Gatteschi, D. (1998). Polyoxometalates: very large clusters nanoscale magnets. *Chem. Rev.* 98: 239–272.

32 Zhang, C., Ma, P., Chen, H. et al. (2011). Synthesis, structure, and properties of a 1-D cerium based on monovacant Keggin-type polyoxotungstate. *J. Coord. Chem.* 64: 2178–2185.

33 Niu, J., Wang, K., Chen, H. et al. (2009). Assembly chemistry between lanthanide cations and monovacant Keggin polyoxotungstates: two types of lanthanide substituted phosphotungstates $[\{(\alpha\text{-}PW_{11}O_{39}H)Ln(H_2O)_3\}_2]^{6-}$ and $[\{(\alpha\text{-}PW_{11}O_{39})Ln(H_2O)(\eta_2,\mu\text{-}1,1)\text{-}CH_3COO\}_2]^{10-}$. *Cryst. Growth Des.* 9: 4362–4372.

34 Fukaya, K. and Yamase, T. (2003). Alkali-metal-controlled self-assembly of crown-shaped ring complexes of lanthanide/$[\alpha\text{-}AsW_9O_{33}]^{9-}$: $[K\subset\{Eu(H_2O)_2(\alpha\text{-}AsW_9O_{33})\}_6]^{35-}$ and $[Cs\subset\{Eu(H_2O)_2(\alpha\text{-}AsW_9O_{33})\}_4]^{23-}$. *Angew. Chem. Int. Ed.* 42: 654–658.

35 Hussain, F., Gable, R.W., Speldrich, M. et al. (2009). Polyoxotungstate-encapsulated Gd_6 and Yb_{10} complexes. *Chem. Commun.* 328–330.

36 Khoshnavazi, R., Naseri, E., Tayamon, S., and Ghiasi Moaser, A. (2011). An evidence for conversion of A-$PW_9O_{34}^{9-}$ derivatives to A-$PW_{10}O_{37}^{9-}$ derivatives. Synthesis and characterization of $[(A\text{-}PW_9O_{34})_2(H_2OM)_3CO_3]^{11-}$ (M = Sm(III), Eu(III) and Gd(III)) and $[(PW_{10}Sm_2O_{38})_4(W_3O_8(H_2O)_2(OH)_4)]^{22-}$ (M = Sm(III) and Gd(III)). *Polyhedron* 30: 381–386.

37 Khoshnavazi, R., Bahrami, L., and Davoodi, H. (2012). Decomposition of the lanthanide-containing sandwich-type polyoxometalates: synthesis and characterization of new multi samarium-containing polyoxometalates. *Inorg. Chim. Acta* 382: 158–161.

38 Kholdeeva, O.A., Timofeeva, M.N., Maksimov, G.M. et al. (2005). Aerobic oxidation of formaldehyde mediated by a Ce-containing polyoxometalate under mild conditions. *Inorg. Chem.* 44: 666–672.

39 Ribeiro, S.O., Nogueira, L.S., Gago, S. et al. (2017). Desulfurization process conciliating heterogeneous oxidation and liquid extraction: organic solvent or centrifugation/water? *Appl. Catal. A* 542: 359–367.

40 Wang, K., Zhang, D., Ma, J. et al. (2012). Three-dimensional lanthanide polyoxometalate organic complexes: correlation of structure with properties. *CrystEngComm* 14: 3205–3212.

41 Li, Z., Li, W., Li, X. et al. (2007). The gadolinium complexes with polyoxometalates as potential MRI contrast agents. *Magn. Reson. Imaging* 25: 412–417.

42 Matsunaga, S., Miyamae, E., Inoue, Y., and Nomiya, K. (2016). β,β-Isomer of open-Wells–Dawson polyoxometalate containing a tetra-iron(III) hydroxide cluster: $[\{Fe_4(H_2O)(OH)_5\}(\beta,\beta\text{-}Si_2W_{18}O_{66})]^{9-}$. *Inorganics* 4: 15.

43 Baker, L.C.W. and Glick, D.C. (1998). Present general status of understanding of heteropoly electrolytes and a tracing of some major highlights in the history of their elucidation. *Chem. Rev.* 98: 3–50.

44 Huang, W., Schopfer, M., Zhang, C. et al. (2008). ^{31}P magic angle spinning NMR spectroscopy of paramagnetic rare-earth-substituted Keggin and Wells–Dawson solids. *J. Am. Chem. Soc.* 130: 481–490.

45 Ueda, T., Nishimoto, Y., Saito, R. et al. (2015). Vanadium(V)-substitution reactions of Wells–Dawson-type polyoxometalates: from $[X_2M_{18}O_{62}]^{6-}$ (X = P, As; M = Mo, W) to $[X_2VM_{17}O_{62}]^{7-}$. *Inorganics* 3: 355–369.

46 Luo, Q.-H., Howell, R.C., Dankova, M. et al. (2001). Coordination of rare-earth elements in complexes with monovacant Wells–Dawson polyoxoanions. *Inorg. Chem.* 40: 1894–1901.

47 Sadakane, M., Ostuni, A., and Pope, M.T. (2002). Formation of 1 : 1 and 2 : 2 complexes of Ce(III) with the heteropolytungstate anion $\alpha_2\text{-}[P_2W_{17}O_{61}]^{10-}$, and their interaction with proline. The structure of $[Ce_2(P_2W_{17}O_{61})_2(H_2O)_8]^{14-}$. *J. Chem. Soc. Dalton Trans.* 63–67.

48 Zhang, C., Bensaid, L., McGregor, D. et al. (2006). Influence of the lanthanide ion and solution conditions on formation of lanthanide Wells–Dawson polyoxotungstates. *J. Clust. Sci.* 17: 389–425.

49 López, X., Carbó, J.J., Bo, C., and Poblet, J.M. (2012). Structure, properties and reactivity of polyoxometalates: a theoretical perspective. *Chem. Soc. Rev.* 41: 7537–7571.

50 Iijima, J. and Naruke, H. (2013). Synthesis and structural characterization of $[CeIV(\alpha_2\text{-}P_2W_{17}O_{61})_2]^{16-}$ in the solid state and in aqueous solution. *J. Mol. Struct.* 1040: 33–38.

51 Boglio, C., Lemière, G., Hasenknopf, B. et al. (2006). Lanthanide complexes of the monovacant Dawson polyoxotungstate $[\alpha_1\text{-}P_2W_{17}O_{61}]^{10-}$ as selective and recoverable Lewis acid catalysts. *Angew. Chem. Int. Ed.* 45: 3324–3327.

52 Kortz, U. (2003). Rare-earth substituted polyoxoanions: $[\{La(CH_3COO)(H_2O)_2(\alpha_2\text{-}P_2W_{17}O_{61})\}_2]^{16-}$ and $[\{Nd(H_2O)_3(\alpha_2\text{-}P_2W_{17}O_{61})\}_2]^{14-}$. *J. Clust. Sci.* 14: 205–214.

53 Peng, Q., Li, S., Wang, R. et al. (2017). Lanthanide derivatives of Ta/W mixed-addendum POMs as proton-conducting materials. *Dalton Trans.* 46: 4157–4160.

54 Chen, W.-C., Jiao, C.-Q., Wang, X.-L. et al. (2019). Self-assembly of nanoscale lanthanoid-containing selenotungstates: synthesis, structures, and magnetic studies. *Inorg. Chem.* 58: 12895–12904.

55 Wang, W., Izarova, N.V., van Leusen, J., and Kögerler, P. (2019). Ce^{III}-functionalized polyoxotungstates: discrete vs extended architectures. *Cryst. Growth Des.* 19: 4860–4870.

56 Ostuni, A. and Pope, M.T. (2000). A large heteropolytungstotetracerate(III) based on a new divacant lacunary derivative of the Wells–Dawson tungstophosphate anion. *C. R. Acad. Sci. – Ser. IIC – Chem.* 3: 199–204.

57 Ostuni, A., Bachman, R.E., and Pope, M.T. (2003). Multiple diastereomers of $[M^{n+}(\alpha_m\text{-}P_2W_{17}O_{61})_2]^{(20-n)-}$ ($M = U^{IV}$, Th^{IV}, Ce^{III}; $m = 1, 2$). Syn- and anti-conformations of the polytungstate ligands in $\alpha_1\alpha_1$, $\alpha_1\alpha_2$, and $\alpha_2\alpha_2$ complexes. *J. Clust. Sci.* 14: 431–446.

58 Fang, X., Anderson, T.M., Benelli, C., and Hill, C.L. (2005). Polyoxometalate-supported Y- and Yb^{III}-hydroxo/oxo clusters from carbonate-assisted hydrolysis. *Chem. Eur. J.* 11: 712–718.

59 Zhao, H.-Y., Zhao, J.-W., Yang, B.-F. et al. (2014). A series of organic–inorganic hybrids based on lanthanide-substituted Dawson-type phosphotungstate dimers and copper–en linkers. *CrystEngComm* 16: 2230–2238.

60 Boglio, C., Lenoble, G., Duhayon, C. et al. (2006). Production and reactions of organic-soluble lanthanide complexes of the monolacunary Dawson $[\alpha_1\text{-}P_2W_{17}O_{61}]^{10-}$ polyoxotungstate. *Inorg. Chem.* 45: 1389–1398.

61 Zhao, H.-Y., Yang, B.-F., and Yang, G.-Y. (2017). Two new 2D organic–inorganic hybrids assembled by lanthanide-substituted polyoxotungstate dimers and copper–complex linkers. *Inorg. Chem. Commun.* 84: 212–216.

62 Granadeiro, C.M., Ferreira, R.A.S., Soares-Santos, P.C.R. et al. (2009). Lanthanopolyoxometalates as building blocks for multiwavelength photoluminescent organic–inorganic hybrid materials. *Eur. J. Inorg. Chem.* 2009: 5088–5095.

63 Yan, B., Liang, R., Zheng, K. et al. (2021). Multinuclear lanthanide-implanted tetrameric Dawson-type phosphotungstates with switchable luminescence behaviors induced by fast photochromism. *Inorg. Chem.* 60: 8164–8172.

64 Lu, Y., Xu, Y., Li, Y. et al. (2006). New polyoxometalate compounds built up of lacunary Wells–Dawson anions and trivalent lanthanide cations. *Inorg. Chem.* 45: 2055–2060.

65 Wei, Z., Wang, J., Yu, H. et al. (2022). Recent advances of Anderson-type polyoxometalates as catalysts largely for oxidative transformations of organic molecules. *Molecules* 27: 5212.

66 Evans, H.T. Jr., (1948). The crystal structures of ammonium and potassium molybdotellurates. *J. Am. Chem. Soc.* 70: 1291–1292.

67 Pope, M.T. (1983). *Heteropoly and Isopoly Oxometalates*. Berlin, Heidelberg: Springer-Verlag.

68 Drewes, D., Limanski, E.M., and Krebs, B. (2004). A series of novel lanthanide polyoxometalates: condensation of building blocks dependent on the nature of rare earth cations. *Dalton Trans.* 2087–2091.

69 An, H., Lan, Y., Li, Y. et al. (2004). A novel chain-like polymer constructed from heteropolyanions covalently linked by lanthanide cations: $(C_5H_9NO_2)_2[La(H_2O)_7CrMo_6H_6O_{24}]\cdot 11H_2O$ (Proline = $C_5H_9NO_2$). *Inorg. Chem. Commun.* 7: 356–358.

70 Dolbecq, A., Dumas, E., Mayer, C.R., and Mialane, P. (2010). Hybrid organic–inorganic polyoxometalate compounds: from structural diversity to applications. *Chem. Rev.* 110: 6009–6048.

71 Blazevic, A. and Rompel, A. (2016). The Anderson–Evans polyoxometalate: from inorganic building blocks via hybrid organic–inorganic structures to tomorrows "Bio-POM". *Coord. Chem. Rev.* 307: 42–64.

72 Pardo, R., Zayat, M., and Levy, D. (2011). Photochromic organic–inorganic hybrid materials. *Chem. Soc. Rev.* 40: 672–687.

73 Preyssler, C. (1970). Existance of 18-tungsto-3-phosphate. *Bull. Soc. Chim. Fr.* 1: 30.

74 Kim, K.-C., Pope, M.T., Gama, G.J., and Dickman, M.H. (1999). Slow proton exchange in aqueous solution. consequences of protonation and hydration within the central cavity of Preyssler anion derivatives, $[|M(H_2O)|\supset P_5W_{30}O_{110}]n$. *J. Am. Chem. Soc.* 121: 11164–11170.

75 Creaser, I., Heckel, M.C., Neitz, R.J., and Pope, M.T. (1993). Rigid nonlabile polyoxometalate cryptates $[ZP_5W_{30}O_{110}]^{(15-n)-}$ that exhibit unprecedented selectivity for certain lanthanide and other multivalent cations. *Inorg. Chem.* 32: 1573–1578.

76 Dickman, M.H., Gama, G.J., Kim, K.-C., and Pope, M.T. (1996). The structures of Europium(III)- and Uranium(IV) derivatives of $[P^5w^{30}o^{110}]_{15-}$: evidence for "cryptohydration". *J. Clust. Sci.* 7: 567–583.

77 Haider, A., Zarschler, K., Joshi, S.A. et al. (2018). Preyssler–Pope–Jeannin polyanions $[NaP_5W_{30}O_{110}]^{14-}$ and $[AgP_5W_{30}O_{110}]^{14-}$: microwave-assisted synthesis, structure, and biological activity. *Z. Anorg. Allg. Chem.* 644: 752–758.

78 Zhang, Z.-M., Yao, S., Li, Y.-G. et al. (2012). Inorganic crown ethers: sulfate-based Preyssler polyoxometalates. *Chem. Eur. J.* 18: 9184–9188.

79 Leclerc, N., Haouas, M., Falaise, C. et al. (2021). Supramolecular association between γ-cyclodextrin and Preyssler-type polyoxotungstate. *Molecules* 26: 5126.

80 Bu, W., Wu, L., and Tang, A.-C. (2004). Polyoxometalates matrixed into surfactants: synthesis, characterizations, and conformations of surfactants. *J. Colloid Interface Sci.* 269: 472–475.

81 Zhang, T., Liu, S., Kurth, D.G., and Faul, C.F.J. (2009). Organized nanostructured complexes of polyoxometalates and surfactants that exhibit photoluminescence and electrochromism. *Adv. Funct. Mater.* 19: 642–652.

82 Zhao, H.-M., Gan, H.-M., Zhao, L., and Su, Z.-M. (2020). Two 2D coordination polymers based on Preyssler anions: synthesis, crystal structures and photoluminescence properties. *Inorg. Chem. Commun.* 113: 107728.

83 Liu, S., Kurth, D.G., Möhwald, H., and Volkmer, D. (2002). A thin-film electrochromic device based on a polyoxometalate cluster. *Adv. Mater.* 14: 225–228.

84 Zhang, T.R., Lu, R., Liu, X.L. et al. (2003). Photochromic polyoxotungstoeuropate $K_{12}[EuP_5W_{30}O_{110}]$/polyvinylpyrrolidone nanocomposite films. *J. Solid State Chem.* 172: 458–463.

85 Hill, C.L., Weeks, M.S., and Schinazi, R.F. (1990). Anti-HIV-1 activity, toxicity, and stability studies of representative structural families of polyoxometalates. *J. Med. Chem.* 33: 2767–2772.

86 Razavi, S.F., Bamoharram, F.F., Hashemi, T. et al. (2020). Nanolipid-loaded Preyssler polyoxometalate: synthesis, characterization and in vitro inhibitory effects on HepG2 tumor cells. *Toxicol. In Vitro* 68: 104917.

87 Pimpão, C., da Silva, I.V., Mósca, A.F. et al. (2020). The aquaporin-3-inhibiting potential of polyoxotungstates. *Int. J. Mol. Sci.* 21: 2467.

88 Xu, Z., Chen, K., Li, M. et al. (2020). Sustained release of Ag^+ confined inside polyoxometalates for long-lasting bacterial resistance. *Chem. Commun.* 56: 5287–5290.

89 Chen, K., Yu, Q., Liu, Y., and Yin, P. (2021). Bacterial hyperpolarization modulated by polyoxometalates for solutions of antibiotic resistance. *J. Inorg. Biochem.* 220: 111463.

90 Dexter, D.D. and Silverton, J.V. (1968). A new structural type for heteropoly anions. The crystal structure of $(NH_4)_2H_6(CeMo_{12}O_{42})\cdot 12H_2O$. *J. Am. Chem. Soc.* 90: 3589–3590.

91 Yamase, T., Naruke, H., and Sasaki, Y. (1990). Crystallographic characterization of the polyoxotungstate $[Eu_3(H_2O)_3(SbW_9O_{33})(W_5O_{18})_3]^{18-}$ and energy transfer in its crystalline lattices. *J. Chem. Soc. Dalton Trans.* 1687–1696.

92 Naruke, H. and Yamase, T. (1998). Crystal structure of $K_{18.5}H_{1.5}[Ce_3(CO_3)(SbW_9O_{33})(W_5O_{18})_3]\cdot 14H_2O$. *J. Alloys Compd.* 268: 100–106.

93 Naruke, H. and Yamase, T. (2002). Size-dependent population of trivalent rare earth cations (RE^{3+}) in $[(RE)_2(H_2O)_2(SbW_9O_{33})(W_5O_{18})_2]^{15-}$, and structural characterization of a luthetium–polyoxotungstate complex $[Lu_3(H_2O)_4(SbW_9O_{33})_2(W_5O_{18})_2]^{21-}$. *Bull. Chem. Soc. Jpn.* 75: 1275–1282.

94 Naruke, H. and Yamase, T. (2002). Synthesis and structure of $Ln(W_5O_{18})$-capped mixed-ligand polyoxotungstolanthanoate $[Ln(W_5O_{18})\{Ln(H_2O)_2(SbW_9O_{33})(W_5O_{18})\}]^{15-}$(Ln = Sm and Er). *Bull. Chem. Soc. Jpn.* 74: 1289–1294.

95 Wang, D., Jiang, J., Cao, M.-Y. et al. (2022). An unprecedented dumbbell-shaped pentadeca-nuclear W-Er heterometal cluster stabilizing nanoscale hexameric arsenotungstate aggregate and electrochemical sensing properties of its conductive hybrid film-modified electrode. *Nano Res.* 15: 3628–3637.

96 Zhang, J., Lai, R.-D., Wu, Y.-L. et al. (2020). High-dimensional polyoxoniobates constructed from lanthanide-incorporated high-nuclear $\{[Ln(H_2O)_4]_3[Nb_{24}O_{69}(H_2O)_3]_2\}$ secondary building units. *Chem. Asian J.* 15: 1574–1579.

97 Liu, J.-C., Wang, J.-F., Han, Q. et al. (2021). Multicomponent self-assembly of a giant heterometallic polyoxotungstate supercluster with antitumor activity. *Angew. Chem. Int. Ed.* 60: 11153–11157.

98 Müller, A., Krickemeyer, E., Meyer, J. et al. (1995). $[Mo_{154}(NO)_{14}O_{420}(OH)_{28}(H_2O)_{70}]^{(25\pm5)-}$: a water-soluble big wheel with more than 700 atoms and a relative molecular mass of about 24000. *Angew. Chem. Int. Ed. Engl.* 34: 2122–2124.

99 Müller, A. and Beugholt, C. (1996). The medium is the message. *Nature* 383: 296–297.

100 Müller, A., Beugholt, C., Bögge, H., and Schmidtmann, M. (2000). Influencing the size of giant rings by manipulating their curvatures: $Na_6[Mo_{120}O_{366}(H_2O)_{48}H_{12}\{Pr(H_2O)_5\}_6]\cdot(\sim 200H_2O)$ with open shell metal centers at the cluster surface. *Inorg. Chem.* 39: 3112–3113.

101 Liu, J.-C., Zhao, J.-W., Streb, C., and Song, Y.-F. (2022). Recent advances on high-nuclear polyoxometalate clusters. *Coord. Chem. Rev.* 471: 214734.

102 Al-Sayed, E. and Rompel, A. (2022). Lanthanides singing the blues: their fascinating role in the assembly of gigantic molybdenum blue wheels. *ACS Nanosci. Au* 2: 179–197.

103 Jia, Y., Zhang, J., Zhang, Z.-M. et al. (2014). Metal-centered polyoxometalates encapsulated by surfactant resulting in the thermotropic liquid crystal materials. *Inorg. Chem. Commun.* 43: 5–9.

104 Ribeiro, S.O., Julião, D., Cunha-Silva, L. et al. (2016). Catalytic oxidative/extractive desulfurization of model and untreated diesel using hybrid based zinc-substituted polyoxometalates. *Fuel* 166: 268–275.

105 Qi, W., Li, H., Wu, L., and Novel, A. (2007). Luminescent, silica-sol–gel hybrid based on surfactant- encapsulated polyoxometalates. *Adv. Mater.* 19: 1983–1987.

106 Zhang, J., Liu, Y., Li, Y. et al. (2012). Hybrid assemblies of Eu-containing polyoxometalates and hydrophilic block copolymers with enhanced emission in aqueous solution. *Angew. Chem. Int. Ed.* 51: 4598–4602.

107 Wei, H., Du, S., Liu, Y. et al. (2014). Tunable, luminescent, and self-healing hybrid hydrogels of polyoxometalates and triblock copolymers based on electrostatic assembly. *Chem. Commun.* 50: 1447–1450.

108 Qi, W. and Wu, L. (2009). Polyoxometalate/polymer hybrid materials: fabrication and properties. *Polym. Int.* 58: 1217–1225.

109 Liu, S. and Tang, Z. (2010). Polyoxometalate-based functional nanostructured films: current progress and future prospects. *Nano Today* 5: 267–281.

110 Clemente-León, M., Coronado, E., Soriano-Portillo, A. et al. (2005). Langmuir–Blodgett films based on inorganic molecular complexes with magnetic or optical properties. *Adv. Colloid Interf. Sci.* 116: 193–203.

111 Liu, S., Kurth, D.G., Bredenkötter, B., and Volkmer, D. (2002). The structure of self-assembled multilayers with polyoxometalate nanoclusters. *J. Am. Chem. Soc.* 124: 12279–12287.

112 Wang, Z., Zhang, R., Ma, Y. et al. (2010). Chemically responsive luminescent switching in transparent flexible self-supporting $[EuW_{10}O_{36}]^{9-}$-agarose nanocomposite thin films. *J. Mater. Chem.* 20: 271–277.

113 Wang, Z., Ma, Y., Zhang, R. et al. (2009). Reversible luminescent switching in a $[Eu(SiW_{10}MoO_{39})_2]^{13-}$-agarose composite film by photosensitive intramolecular energy transfer. *Adv. Mater.* 21: 1737–1741.

114 Wang, B.-H. and Yan, B. (2019). Tunable multi-color luminescence and white emission in lanthanide ion functionalized polyoxometalate-based metal–organic frameworks hybrids and fabricated thin films. *J. Alloys Compd.* 777: 415–422.

115 Denny, M.S., Kalaj, M., Bentz, K.C., and Cohen, S.M. (2018). Multicomponent metal–organic framework membranes for advanced functional composites. *Chem. Sci.* 9: 8842–8849.

116 Mirante, F., Salimian, M., Marques, P.A.A.P. et al. (2022). Polyoxometalate-doped electrospun nanofiber mats as active catalysts for the production of clean fuels under solvent-free systems. *Sustainable Energy Fuels* 6: 4681–4691.

117 Zhou, Y., Chen, G., Long, Z., and Wang, J. (2014). Recent advances in polyoxometalate-based heterogeneous catalytic materials for liquid-phase organic transformations. *RSC Adv.* 4: 42092–42113.

118 Jia, M. and Thiel, W.R. (2002). Oxodiperoxo molybdenum modified mesoporous MCM-41 materials for the catalytic epoxidation of cyclooctene. *Chem. Commun.* 2392–2393.

119 Xiong, J., Zhu, W., Ding, W. et al. (2014). Phosphotungstic acid immobilized on ionic liquid-modified SBA-15: efficient hydrophobic heterogeneous catalyst for oxidative desulfurization in fuel. *Ind. Eng. Chem. Res.* 53: 19895–19904.

120 Choi, M., Heo, W., Kleitz, F., and Ryoo, R. (2003). Facile synthesis of high quality mesoporous SBA-15 with enhanced control of the porous network connectivity and wall thickness. *Chem. Commun.* 1340–1341.

121 Omwoma, S., Chen, W., Tsunashima, R., and Song, Y.-F. (2014). Recent advances on polyoxometalates intercalated layered double hydroxides: from synthetic approaches to functional material applications. *Coord. Chem. Rev.* 258–259: 58–71.

122 Liu, K., Yao, Z., and Song, Y.-F. (2015). Polyoxometalates hosted in layered double hydroxides: highly enhanced catalytic activity and selectivity in sulfoxidation of sulfides. *Ind. Eng. Chem. Res.* 54: 9133–9141.

123 Wang, X., Chen, W., and Song, Y.-F. (2014). Directional self-assembly of exfoliated layered europium hydroxide nanosheets and $Na_9EuW_{10}O_{36}\cdot 32H_2O$ for application in desulfurization. *Eur. J. Inorg. Chem.* 2014: 2779–2786.

124 Jia, Y., Zhao, S., and Song, Y.-F. (2014). The application of spontaneous flocculation for the preparation of lanthanide-containing polyoxometalates intercalated layered double hydroxides: highly efficient heterogeneous catalysts for cyanosilylation. *Appl. Catal. A* 487: 172–180.

125 Li, T., Wang, Z., Chen, W. et al. (2017). Rational design of a polyoxometalate intercalated layered double hydroxide: highly efficient catalytic epoxidation of allylic alcohols under mild and solvent-free conditions. *Chem. Eur. J.* 23: 1069–1077.

126 Sousa, F.L., Pillinger, M., Sá Ferreira, R.A. et al. (2006). Luminescent polyoxotungstoeuropate anion-pillared layered double hydroxides. *Eur. J. Inorg. Chem.* 2006: 726–734.

127 Omwoma, S., Lagat, S.C., and Lalah, J.O. (2018). Fine tuning the microenvironment of $[EuW_{10}O_{36}]^{9-}$ anion leads to the large enhancement of the red light luminescence. *J. Lumin.* 196: 294–301.

128 Zhu, Q.-L. and Xu, Q. (2014). Metal–organic framework composites. *Chem. Soc. Rev.* 43: 5468–5512.

129 Piscopo, C.G., Granadeiro, C.M., Balula, S.S., and Bošković, D. (2020). Metal-organic framework-based catalysts for oxidative desulfurization. *ChemCatChem* 12: 4721–4731.

130 Granadeiro, C.M., Silva, P., Saini, V.K. et al. (2013). Novel heterogeneous catalysts based on lanthanopolyoxometalates supported on MIL-101(Cr). *Catal. Today* 218–219: 35–42.

131 Ribeiro, S., Granadeiro, C.M., Silva, P. et al. (2013). An efficient oxidative desulfurization process using terbium-polyoxometalate@MIL-101(Cr). *Cat. Sci. Technol.* 3: 2404–2414.

132 Granadeiro, C.M., Nogueira, L.S., Julião, D. et al. (2016). Influence of a porous MOF support on the catalytic performance of Eu-polyoxometalate based materials: desulfurization of a model diesel. *Cat. Sci. Technol.* 6: 1515–1522.

133 Juan-Alcañiz, J., Ramos-Fernandez, E.V., Lafont, U. et al. (2010). Building MOF bottles around phosphotungstic acid ships: one-pot synthesis of bi-functional polyoxometalate-MIL-101 catalysts. *J. Catal.* 269: 229–241.

134 Férey, G., Mellot-Draznieks, C., Serre, C. et al. (2005). A chromium terephthalate-based solid with unusually large pore volumes and surface area. *Science* 309: 2040–2042.

135 Salomon, W., Dolbecq, A., Roch-Marchal, C. et al. (2018). A multifunctional dual-luminescent polyoxometalate@metal-organic framework EuW_{10}@UiO-67 composite as chemical probe and temperature sensor. *Front. Chem.* 6: 425.

136 Viravaux, C., Oms, O., Dolbecq, A. et al. (2021). Temperature sensors based on europium polyoxometalate and mesoporous terbium metal–organic framework. *J. Mater. Chem. C* 9: 8323–8328.

137 Abdelkader-Fernández, V.K., Fernandes, D.M., Balula, S.S. et al. (2020). Advanced framework-modified POM@ZIF-67 nanocomposites as enhanced oxygen evolution reaction electrocatalysts. *J. Mater. Chem. A* 8: 13509–13521.

138 Abdelkader-Fernández, V.K., Fernandes, D.M., Balula, S.S. et al. (2022). Unveiling the structural transformations of the $PW_{11}Co$@ZIF-67 nanocomposite induced by thermal treatment. *Dalton Trans.* 51: 17844–17857.